Original Paper

Landslides
DOI 10.1007/s10346-025-02568-x
Received: 13 November 2024
Accepted: 26 June 2025

Luigi Guerriero · Maximillian Van Wyk de Vries · Holly Hourston · Alessandro Novellino · Domenico Calcaterra · Diego Di Martire · Nicola Sciarra · Mirko Francioni

Earthquakes and rainfall accelerating deep-seated landslides toward failure: significance of combined use of InSAR and feature tracking in landslide analysis

Abstract Deep-seated landslides are found across various geological settings, with their velocity influenced by processes such as rainfall infiltration and earthquakes shaking, which alter pore pressure and shear stress at the landslide base. This paper examines the Borrano and Ponzano landslides in Abruzzo, central Italy, as representative examples of deep-seated landslides. Our analysis focuses on their geometry, mechanisms, and velocity changes using field, subsurface, and remote sensing. Both landslides, involving Laga Formation rocks, feature a concave basal sliding surface and exhibit rotational sliding with continuous movement since at least 2015. Displacement rates exceeded 10 mm/year between 2015 and 2022, with the Ponzano landslide moving 15 m in a few days during a slip event in February 2017. Time series analysis shows a substantial velocity change at both landslides following the August 24, 2016, earthquake and 2 months of above-average rainfall, with the Ponzano landslide slipping 15 m 6 months later. While our data does not provide a conclusive origin for this rapid slip event, the earlier changes suggest that earthquakes and rainfall can perturb landslide motion, possibly driving strain-induced material weakening and eventual failure.

Keywords Landslides · Kinematics · Catastrophic failure · InSAR · Feature tracking · Earthquake

Introduction

Deep-seated landslides occur worldwide across a variety of geological environments (Baron et al. 2004; Roering et al. 2005; Brideau et al. 2009; Kojima et al. 2015; Březný and Pánek 2017; Pappalardo et al. 2018; Arai and Chigira 2019; Esposito et al. 2021; Guerriero et al. 2021). Their initiation is commonly related to rainfall infiltration and earthquake shaking (Chigira and Yagi 2006; Zhi et al. 2016; Chen et al. 2017; Confuorto et al. 2017; Nguyen et al. 2020), but marine erosion, sprawl of urbanized areas, weakening of landslide material due to long-term alteration, and land-use change have also been identified as potential triggering factors (Cevasco et al. 2018; Dille et al. 2019, 2022). Blasting, tunneling, and excavation can also contribute to this process (Sun et al. 2012), even if, in some cases, deep-seated landslide initiation has not been associated with a specific trigger. Deep-seated landslide motion can be modulated by pore pressure fluctuations at the landslide basal and lateral slip surfaces and variation in weight caused by water infiltration (Iverson 2005; Schulz et al. 2009; Van Asch et al. 2009; Handwerger et al. 2015; Schulz et al. 2017; Jiang et al. 2018). Earthquakes can be responsible for transient acceleration due to a temporal increase in shear stress caused by seismic loading and eventual pore-water pressure build-up (Newmark 1965; Sassa et al. 1996; Wasowski et al. 2002; Lacroix et al. 2015). Although slow-moving or intermittent kinematics can persist over the long term, these landslides can suddenly fail catastrophically (Chigira 2009). Intense rainfall, earthquakes, and undrained loading by superimposed landslides can be responsible for catastrophic evolution (Chigira 2009; Booth et al. 2018). Under specific circumstances, long-term creep can drive a slope toward failure (Petley and Allison 1997; Guerriero et al. 2022).

Tracking and understanding deep-seated landslide kinematics is critical for assessing their hazard and risk. Being characterized by velocities that range from millimeters per year to meters per second (in case of catastrophic failure, i.e., very slow to extremely rapid; Hungr et al. 2014) and often affecting significantly large areas, monitoring spatial pattern and rate of surface displacement can be a challenging task that benefits from the integration of multiple satellite-based techniques. Over the last three decades, Differential Interferometric Synthetic Aperture Radar (DInSAR) has emerged as a valuable tool for landslide displacement monitoring from slope to regional scale (Antonello et al. 2004; Colesanti and Wasowski 2006; Schlogel et al. 2015; Di Martire et al. 2016, 2017; Squarzoni et al. 2020; Manconi 2021). This technique has the potential to support low-rate displacement tracking applications and mapping and, due to the characteristics of the sensors, it is able to work in all-weather and day and night conditions. A major limitation of this technique is related to its inability to track north–south and high-rate displacement, especially in the case of high-resolution analysis (Ferretti et al. 2001). Some of these limitations can be overcome by optical feature tracking (also known as pixel offset tracking or particle image velocimetry) which is less affected by vegetation and displacement orientation and is less affected by decorrelation (Stumpf et al. 2017; Guerriero et al. 2020; Van Wyk de Vries et al. 2024). Since DInSAR is suitable for slow-rate displacement monitoring and feature tracking is suitable for monitoring faster motion, a combination of both techniques may provide the most comprehensive opportunity for landslide displacement tracking, although one or both may not perform effectively over some areas (e.g. Dille et al. 2021; Van Wyk de Vries et al. 2021, 2024).

Deep-seated landslides of variable size and age are distributed across Italy's Apennine mountains. Many of them occur in

structurally complex flyschoid formations (Esu 1977) and underlie or are adjacent to human settlements, inducing damage to buildings and infrastructures. This interaction is often related to their extremely slow displacement rate and eventual intermittent nature since, in these conditions, they can remain unrecognized for decades, allowing settlements to be built on them. This is the case of many villages of the Campania Region that, every year, suffer diffuse damage induced by active deep-seated landslides (Di Martire et al. 2013; Guerriero et al. 2019). Deep-seated landslides involving structurally complex flyschoid formations are often controlled by lithostratigraphic and structural settings that predispose slopes to landslide development (Baron et al. 2004; Martino et al. 2004; Pinto et al. 2016; Břežný and Pánek 2017). The presence of thin-bedded weak claystone underlining thick-bedded sandstone, significant fracturing, and the presence of an association of faults and folds are examples of elements controlling deep-seated landslide development and evolution.

The Borrano and Ponzano landslides are two examples of deep-seated landslides affecting structurally complex flyschoid formations (Esu 1977) and involving villages (Borrano and Ponzano) of the Appennine range of central Italy (Fig. 1). The existence of the two landslides was discovered around 2003, when small damages were spotted in some of the buildings of the villages. The first monitoring systems applied in the two areas highlighted the slow-moving behavior of the two landslides. However, with years, the slow-moving Borrano landslide kept damaging settlements and infrastructures and recently caused many families to be evacuated as a consequence of structural damage to buildings induced by long-term displacement. This landslide is currently monitored through multiple instrumentation stations, and landslide risk is assessed in near real-time through a monitoring-based early-warning system. Diversely, the Ponzano landslide changed behavior on February 12, 2017, with an extraordinary failure of the landslide and displacements moving from few centimeters per years to meters per day, destroying part of the village (Solari et al. 2018). Immediately after the event, many families of the village were evacuated, and a monitoring system consisting of repeated UAV surveys and near-real-time topographic measurements was adopted and worked between February and June 2017 and February and August 2017, respectively (Allasia et al. 2019). Both landslides occur along a west-trending hillslope characterized, at landslide locations, by a similar geologic setting, morphology, and elevation. In this context, predisposing conditions facilitating catastrophic failure of the Ponzano landslide might drive the Borrano landslide toward failure in the future. On this basis, in this paper, the Borrano and Ponzano landslides are analyzed with the aim of contributing to a better understanding of conditions and mechanisms driving catastrophic failure of deep-seated landslides involving structurally complex formations as well as documenting their kinematics prior (both the Borrano and Ponzano landslides), during, and after the failure (limited to the Ponzano landslide). In this perspective, data from field observations, subsurface exploration, laboratory testing, borehole inclinometers, DInSAR data, and feature tracking method are consistently used to unravel landslides geometry, mechanisms, and velocity variation. Rainfall and earthquake data are considered for the interpretation of factors promoting catastrophic failure. The significance of this analysis is related to the lesson learned from the Ponzano surging event and its application to the Borrano landslide and is also related to its contribution in underlining the need for a slope-scale engineering-geological model guiding interpretation of mechanism and kinematics of deep-seated landslide as well as the need, for landslides, of integrating available DInSAR data and feature tracking methods in order to derive reliable data describing kinematics prior, during, and after failure.

Study area

The Borrano and Ponzano landslides are two large deep-seated landslides located in the municipality of Civitella del Tronto, Abruzzo Region, Italy, and affecting the villages of Borrano and Ponzano (Fig. 1). The two landslides involve east-trending slopes mostly formed by Cenozoic fine-grained flyschoid materials described as the Laga formation (Upper Messinian), which is characterized by an association of clayey marls, marly clays, and sandstones (Fig. 2). In particular, in the study area, the Laga formation is characterized by multiple lithofacies and levels of regional stratigraphic significance, including the LAG6e, LAG6d, and LAG6c. These lithofacies, highlighted in the geological map of Fig. 2, are characterized by a variable arenite/pelite ratio, moving from the mainly arenite lithofacies LAG6e to the predominantly pelite LAG6c. The Villa Romita and Colle Torrone stratigraphic levels crop out at the western sector of the study area. In the eastern sector, the Laga formation is overlaid by the Vomano formation, mainly represented by associations of marls and clays, and locally covered by recent alluvial, colluvial, and landslide deposits. From a structural point of view, the area is characterized by eastward and generally > 40° dipping beds of Cenozoic rocks of the Laga formation and local NE-SW oblique faults. This eastward monoclinal condition is consistently related to the Cenozoic and Neozoic compressive tectonics, responsible for the development of the Abruzzi mountainous belt, and for the subsequent uplift and eastward tilting. This geological setting creates conditions for a local gently sloping (i.e., ~ 10°) and smooth longitudinal shape of slopes, especially toward the Salinello River valley. Local higher slope values are present where sandstones crop out (Cantalamessa and Di Celma 2004). In the study area, the slopes are quite significantly developed in length (i.e., up to ~ 2 km) and characterized by a sub-dendritic pattern of the hydrographic network.

It is also important to note that the study area is located in a seismic areas of the Apennine Chain characterized by a PGA with 10% probability to be exceeded in 50 years around 0.2 (Meletti et al. 2021). More in detail, it is less than 60 km far from the epicenters and the earthquake faults of the 2016–2017 earthquakes occurred in central Italy, with the major events characterized by a $6.0 < Ms < 6.5$ magnitude (Chiaraluce et al. 2017). Besides causing diffuse damage to settlements and surface ruptures next to the earthquake faults (Carboni et al. 2022), the 2016–2017 earthquakes either induced or reactivated many landslides (Martino et al. 2019; Forte et al. 2021), potentially including the Borrano and Ponzano landslides. The Borrano landslide, affecting the slope from 240 to 440 m asl, is characterized by a smooth, slow, and continuous movement which has caused remarkable damages to infrastructure since 2017. The Ponzano landslide, affecting the slope from 200 to 400 m asl, had an abrupt reactivation on February 12, 2017, that partially destroyed the Ponzano village (Solari et al. 2018; Calista et al. 2019).

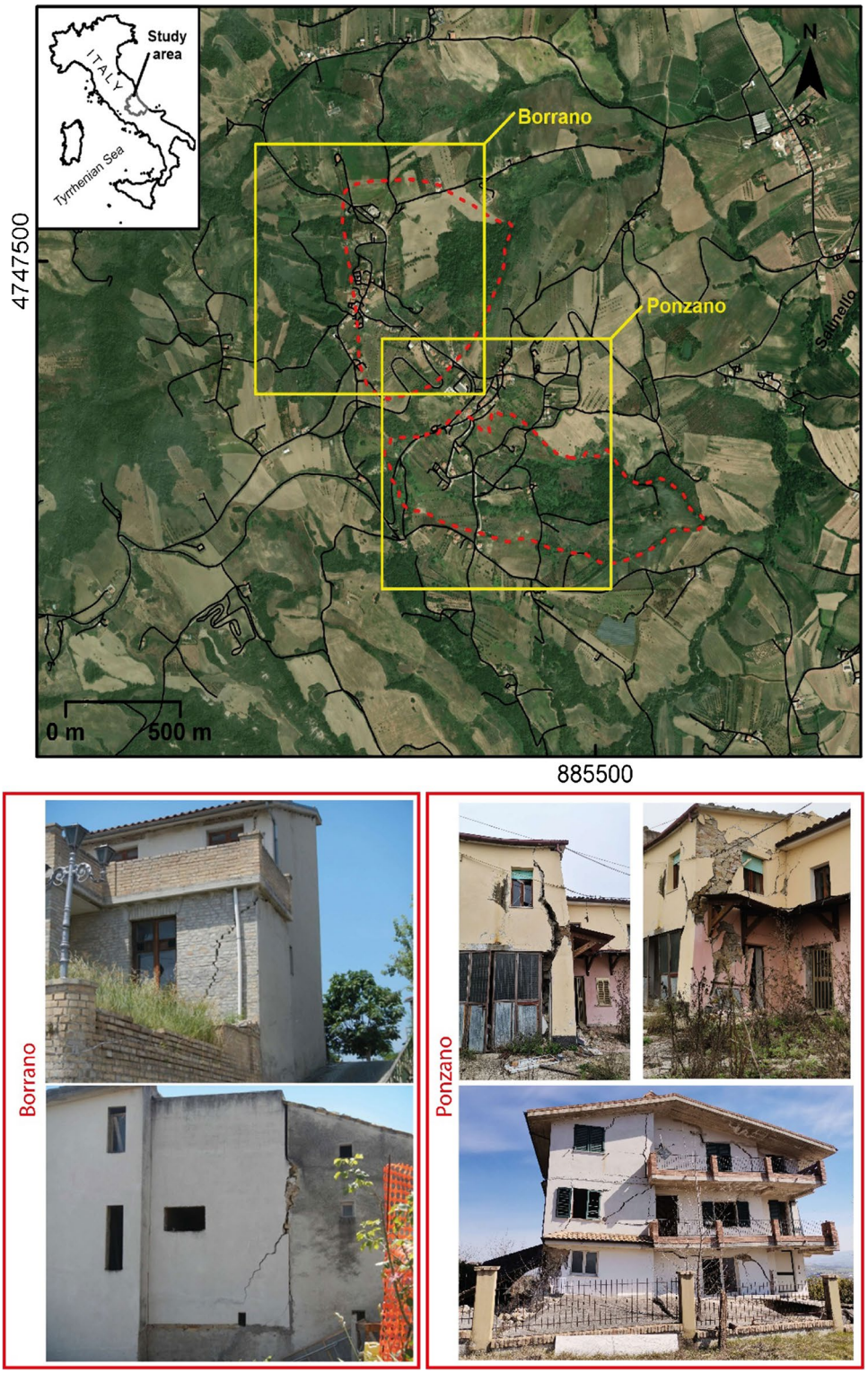

Fig. 1 Map showing position and boundaries (red dashed lines) of the Borrano and Ponzano landslides and associated pictures depicting their effects in settlements. Yellow polygons depict areas of interest for either the Borrano and Ponzano landslides. UTM 32 N coordinates are shown at map edges

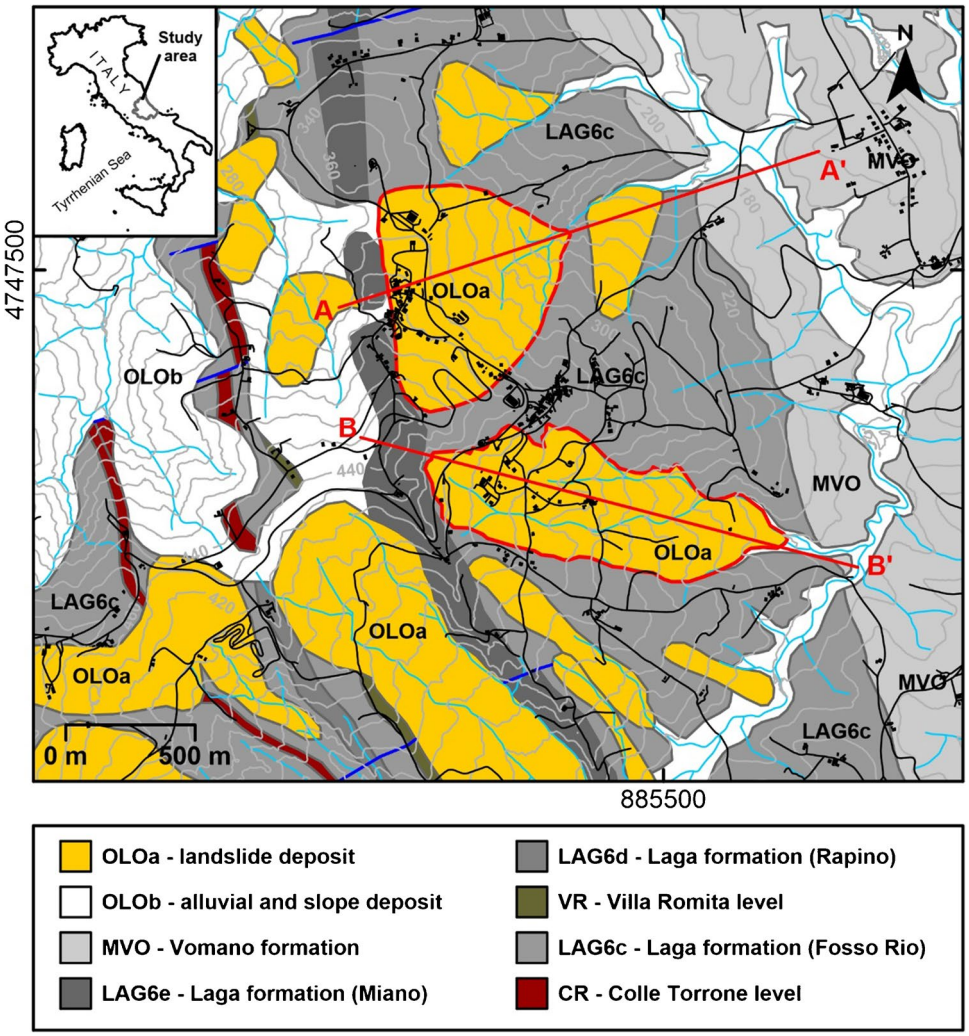

Fig. 2 Geological map of the study area depicting formations cropping out as well as major landslides. Inset map shows the position of the study area. Major urban areas are indicated by black artworks. UTM 32 N coordinates are shown at map edges

Methods

To contribute to a better understanding of conditions and mechanisms driving catastrophic failure of deep-seated landslides involving structurally complex formations as well as documenting their kinematics prior, during, and after the failure, an integrated method, consisting of collection of available subsurface exploration data, material properties, and monitoring data including borehole inclinometers readings and available DInSAR data from European Ground Motion Service (EGMS—https://egms.land.copernicus.eu/), field mapping, feature tracking of Sentinel-2 imagery, and displacement rate time series analysis, was used. Data from field mapping, including position and deformational style of landslide margins, available subsurface exploration data, and material properties, were used to reconstruct the engineering-geological model of the Borrano and Ponzano landslides. Available EGMS data and data derived from feature tracking of Sentinel-2 imagery were used to track slow movements of the landslides and faster movements of the Ponzano landslide during failure. Time series analysis helped in deciphering the influence of rainfall events and earthquakes on the transition between slow movement and catastrophic slope failure. Figure 3 shows the described methodological work flow and is worth here to point out the importance of integrating different survey and analysis techniques, with particular focus on the use of feature tracking analysis in fast-moving phenomena.

Landslides geometry and engineering-geological model reconstruction

The engineering-geological models of the Borrano and Ponzano landslides, depicting their 3D geometry as well as distribution of geologic materials and their properties, were reconstructed on the basis of data deriving from field mapping of landslide margins, borehole logs, borehole inclinometric monitoring data, seismic refraction profiles, electrical resistivity tomography, and laboratory testing on samples taken during borehole drilling (see Fig. 4 for location). Landslide margins geometry was reconstructed considering position and characteristics of surface deformational structures

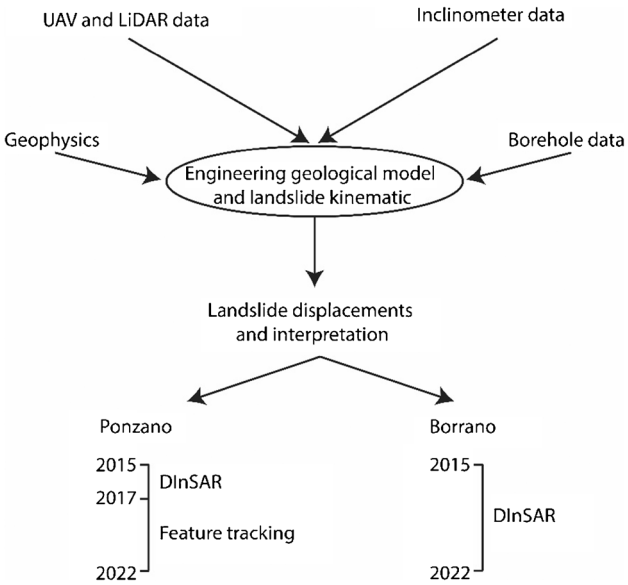

Fig. 3 Methodological work flow

indicating stretching, shortening, and relative movement of the landslide (Fleming and Johnson 1989; Baum and Fleming 1991; Guerriero et al. 2016, 2017). For both landslides, such structures were locally mapped in the field using GNSS kinematic technique and through the interpretation of an UAV-derived orthoimage. Morphological elements such as drainage channel anomalies, back-tilting surface, and surface hummocks indicating potential landslide-induced deformation were mapped as well. Data from subsurface exploration and monitoring were considered to reconstruct the cross-sectional geometry of the Borrano and Ponzano landslides. At Borrano, the position at depth of the basal-slip surface derived by interpretation of six boreholes log completed between 2018 and 2023 (i.e., position of slickensided surfaces and damaged material) and inclinometric monitoring data, acquired between 2018 and 2019 at three inclinometers (S1, S2, and S3) installed within the urban area of Borrano, were used in association to data derived by the interpretation of distribution of P-wave and electrical resistivity at depth along geophysical profiles. At Ponzano, the position of the basal slip surface at depth derived by interpretation of five boreholes log completed in 2022 (i.e., position of slickensided surfaces and damaged material) and inclinometric monitoring data, acquired between 2022 and 2023 at two inclinometers (S2 and S3) installed below from the urban area of Ponzano, were considered in association to data derived by the interpretation of distribution of P-wave at depth along three geophysical profiles. Material properties data were derived by laboratory testing on samples taken during boreholes drilling at variable depths. Especially, specific gravity, grain size distribution, and unit weight were estimated (ASTM Standards, D 854, D 422 and D 2937, respectively). In addition, direct shear tests were completed to determine both peak and residual drained shear strength of materials and corresponding strength parameters (ASTM Standards D 3080).

Slow movement tracking from EGMS data

The slow movement of the Borrano and Ponzano landslides was tracked using EGMS data (Crosetto et al. 2021). Specifically, Persistent Scatterers (PS) data depicting average Line of Sight (LoS) displacement rate between 2015 and 2022 in ascending and descending acquisition orbits were used to identify actively deforming zones as a function of their ground deformation rate. Only ground deformation rates higher than 2 mm/year were considered indicative of actively deforming zones, for both look geometries and for westward and eastward movement directions. After the identification, significant PS were selected in actively deforming zones of the landslides, and time series were generated and analyzed for landslide displacement tracking. For significant PS identification, the spatial consistence of the velocity, its modulus, and the overall position in comparison with landslide sectors (i.e., head, transport zone, and

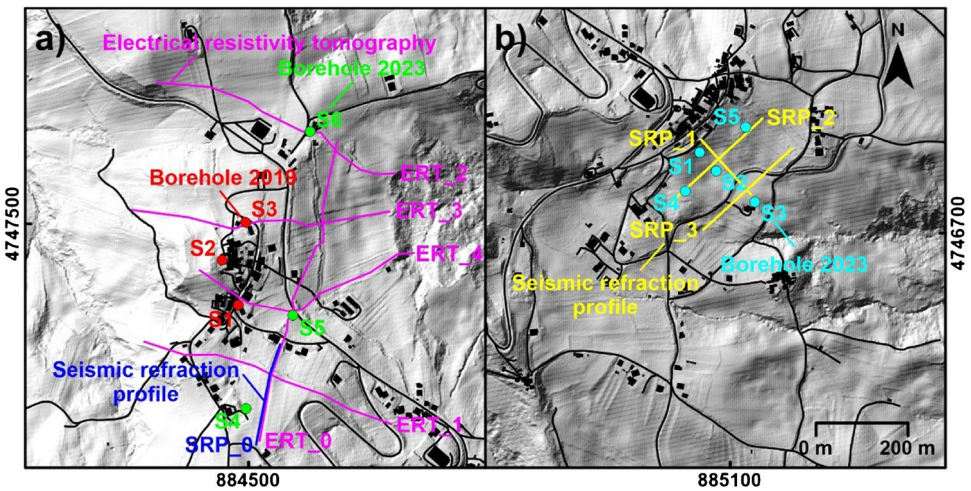

Fig. 4 Maps showing the location of available boreholes, seismic refraction profiles, and electrical resistivity tomography considered for the reconstruction of the 3D geometry and engineering-geological models of the **a** Borrano and **b** Ponzano landslides. Maps extent corresponds to yellow polygons of Fig. 1. UTM 32 N coordinates are shown at maps' edges

toe) were considered. Displacement time series derived by selected groups of PS located at the upper sector of the landslides, extracted as the median of the horizontal and vertical components of the DInSAR time series (derived on the basis of direction cosines of the ascending and descending displacement vectors), were analyzed through the additive Seasonal Trend LOESS (STL) decomposition model (Cleveland et al. 1990). This model is able to perform additive decomposition of the data through a sequence of applications of the LOESS smoother, through the application of a local weighted polynomial regressions at each point in the time series. This model was selected because of its capacity to deal with long time series and its ability of working in presence of significant noise and outliers, as potentially expected for DInSAR time series. The trend components of the STL results have been further analyzed with PieceWise Linear Functions (PWLF) as recently done by Rygus et al. (2023). PWLF are used to detect sudden acceleration or deceleration in the displacements and their initiation point. From the trend component of the STL analysis, major breakpoints identifying displacement rate change were extracted and compared with the timing of occurrence of major known rainfall and earthquake events in order to unravel the conditions and factors controlling landslide kinematics and potential acceleration driving catastrophic failure of the Ponzano landslide. From this perspective, rainfall data from the meteorological station of Civitella del Tronto, 2 km away from the study sites, and available earthquake data depicting position and magnitude of events occurred during the 2016–2017 Central Italy earthquake sequence were considered. Since landslide thickness ranges from ~ 15 to ~ 50 m and expected maximum hydraulic diffusivity of fine-grained landslide material should be ~ 1×10^{-4} (Iverson and Major 1987; Schulz et al. 2009), minimum timescale for landslide response due to pore pressure generation by rain infiltration can be estimated at ~ 30 days (Iverson 2000). On this basis, monthly rainfall data were considered for the analysis.

Displacement estimate from Feature Tracking analysis of Sentinel-2 imagery

Due to the limitations of tracking rapid displacement using DInSAR data, the motion of the Ponzano landslide was evaluated using an optical feature-tracking workflow. This workflow is a modified version of the Glacier Image Velocimetry (GIV) toolbox, originally developed for mapping ice flow speeds (Van Wyk de Vries and Wickert 2021), with the landslide-oriented modifications described in Van Wyk de Vries et al. (2024). While no site-specific validation was performed in this case, the GIV workflow has previously been benchmarked against independent and ground-based measurements (Van Wyk de Vries et al. 2024), demonstrating robust performance in comparable applications.

Feature tracking was applied to Sentinel-2 Level-1C imagery, specifically using Band 8 (near-infrared, 833 nm), which provides a 10 m spatial resolution. We assembled a stack of Sentinel-2 images spanning 2016–2017 and manually filtered out all scenes with visible cloud cover. To enhance surface pattern contrast and uniqueness, an orientation filter was applied to the images (Van Wyk de Vries and Wickert 2021). This yielded 36 usable images over the 2-year period. All possible image pairs with temporal separations greater than 9 months were constructed. This bound balances the need for detectable displacement in slow-moving landslides with the need to avoid excessive temporal smoothing that may mask rapid events. No upper bound on temporal separation was imposed, as most of the surface was expected to remain coherent over the 2-year interval, except in cases of anthropogenic disturbance or landslide motion. The detection limit of this workflow depends on image resolution, surface texture, and temporal stacking. For Sentinel-2 imagery, reported detection limits range from 0.13–1.3 m a^{-1} for a 9-month baseline to 0.05–0.5 m a^{-1} for a 2-year baseline (Van Wyk de Vries et al. 2024; Stumpf et al. 2017).

We employed a single-pass chip-wise cross-correlation algorithm with a 16-pixel window size and 50% window overlap, yielding an effective spatial resolution of ~ 80 m. This configuration reduces noise while preserving sub-100 m resolution. A single-pass algorithm was chosen over the default GIV three-tier multipass routine because expected integer displacements are near zero, eliminating the benefit of coarse-to-fine refinement (Van Wyk de Vries and Wickert 2021). Additional modifications to the GIV algorithm and processing chain are described in Van Wyk de Vries et al. (2024).

Two displacement scenarios were considered: (i) temporally distributed displacement ("constant velocity") occurring over part or all of the time series, and (ii) a single discrete event ("single slip event") with no motion before or after. This distinction ensures appropriate processing and avoids bias—e.g., a near-zero median velocity estimate when few image pairs span a single event. For the constant velocity case, displacements were converted to velocity vectors by dividing by the temporal baseline and scaling by image resolution. For the single-event case, displacements were retained in their raw form and scaled only by image resolution.

To remove false matches, all pixels with a cross-correlation peak ratio (ratio of primary to secondary peak) < 1.5 were excluded (Van Wyk de Vries and Wickert 2021). This signal-to-noise ratio filter also eliminates areas affected by decorrelation due to vegetation change (e.g., crop planting). Finally, median scene-wide velocities or displacements in both E–W and N–S directions were removed to correct for systematic georeferencing offsets. These corrections were applied independently to each velocity component to prevent transformation of residual noise.

Results

Landslide geometry and engineering-geological model

Landslide geometry and engineering-geological model were extracted by the integration of borehole and inclinometer data, field and UAV surveys, and geotechnical and geophysical data. While at Borrano tension cracks and normalfault-like scarps indicating stretching of the upper sector of the landslide prevailed (Fig. 5), at Ponzano, tension cracks and normalfault-like scarps indicating stretching of the upper sector of the landslide were associated with strike-slip fault-like structures, indicating relative movement along the margin of the central sector of the landslide and thrust fault-like structures indicating compression at the landslide toe (Fig. 6). In both case studies, borehole data, which reached up to 80 m in depth, highlighted a very similar stratigraphy with a bedrock characterized by a sequence of pelitic-arenaceous layers within the Laga Formation, dipping 40–60° toward ENE. Colluvial/alluvial deposits cover the bedrock with thickness ranging from a few to 15 m. This agrees with geophysical data, showing the first reflectors at a depth

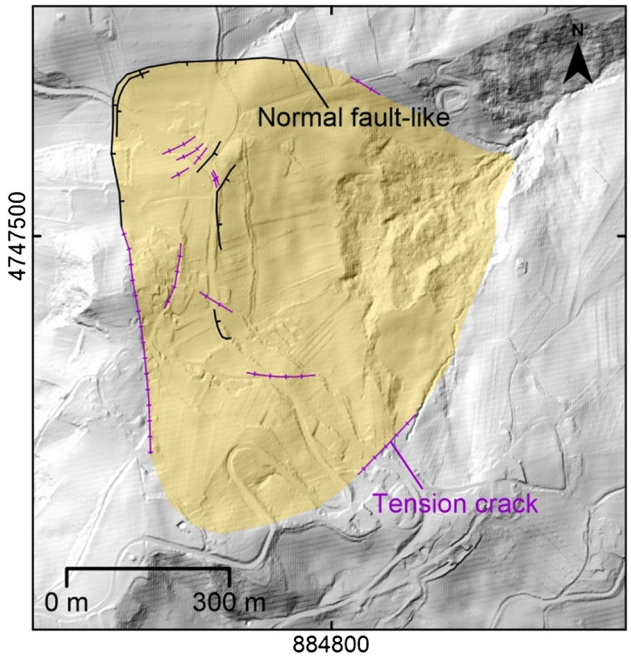

Fig. 5 Deformational features identified at the surface of Borrano landslide

ranging from a few to 20 m (related to the alluvial deposits and sandy layers) and the bedrock, with $V_P > 1000$ m s^{-1}, below that. The analysis of inclinometer data shows that there are two different deformation surfaces at 10–15 m and 40–50 m in depth, respectively. The use of borehole data played a key role in the definition of lithological and geotechnical characteristics of geological layers. The thickness of colluvial/alluvial deposits, in fact, did not allow the finding of good bedrock outcrops in the study areas. Figure 7 shows the geometry of landslides gathered from field, LiDAR, and UAV survey, and the geological sections A-A' and B-B' developed integrating borehole and inclinometer data. From a geotechnical point of view, laboratory tests carried out on samples taken from the pelitic-arenaceous layers of the Laga Formation indicate a particle size distribution with 44% of silt, 32% of clay, and 24% of sand, as well as an effective cohesion and friction angle of 15.4 kPa and 28° for materials of both landslides.

Displacement and velocity at Borrano and Ponzano, prior and after the failure of February 12, 2017

Figure 8 shows distribution of available ascending and descending PS data derived from the EGMS and depicting the average surface velocity of the Borrano and Ponzano landslide between 2015 and 2022. For both landslides, PSs are mainly distributed around the upper and central sectors, with the Borrano landslide having approximately 8 times more PS than Ponzano (i.e., Borrano upper: ~ 200 PSs; Ponzano upper: ~ 20 PSs; Borrano central: ~ 80 PSs; Ponzano central ~ 20 PSs in both geometries). This is related to the absence of natural reflectors at the lower sector of both landslides. Overall, while the upper sector of the Borrano landslide exhibits higher and spatially coherent ascending velocity in comparison with the Ponzano landslide (< − 10 mm/yr vs between − 5 and − 10 mm/yr), the upper sectors of the Ponzano landslide move locally faster than the same zone of the Borrano landslide in terms of descending velocity (> 10 mm/yr vs between 5 and 10 mm/yr; Fig. 8). The central sector of both landslides exhibits similar descending velocities (between 5 and 10 mm/yr). In addition, moving from the axis toward the landslide margin, the change in ascending velocity is higher for the Ponzano landslide, while the change in descending velocity is greater for the Borrano landslide. Available PS distribution also indicates either a local smooth or abrupt transition between the non-moving zone and velocity between 5 and 10 mm/yr near the upper boundary of the Borrano landslide and the left margin of the Ponzano landslide. In both

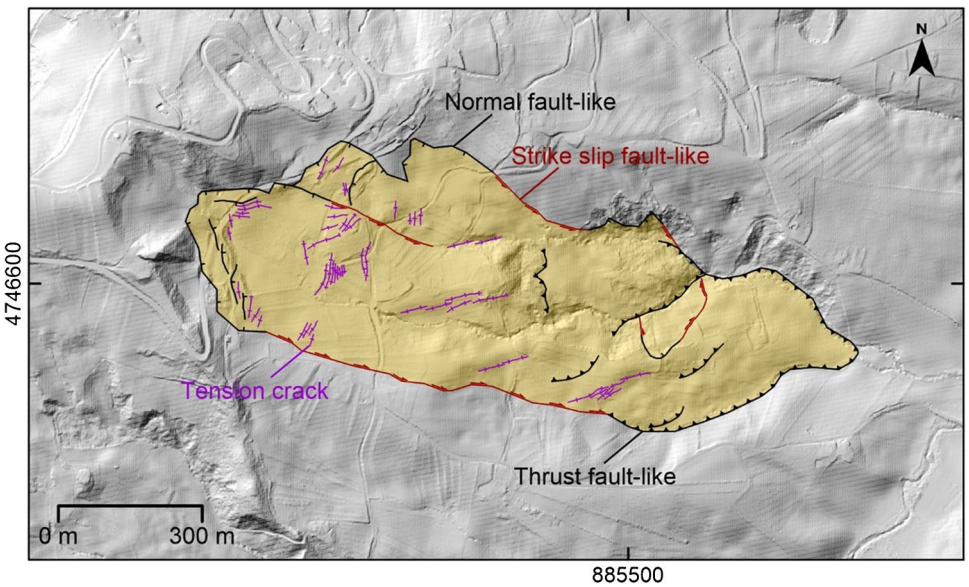

Fig. 6 Deformational features identified at the surface of Ponzano landslide after the catastrophic failure of February 12, 2017

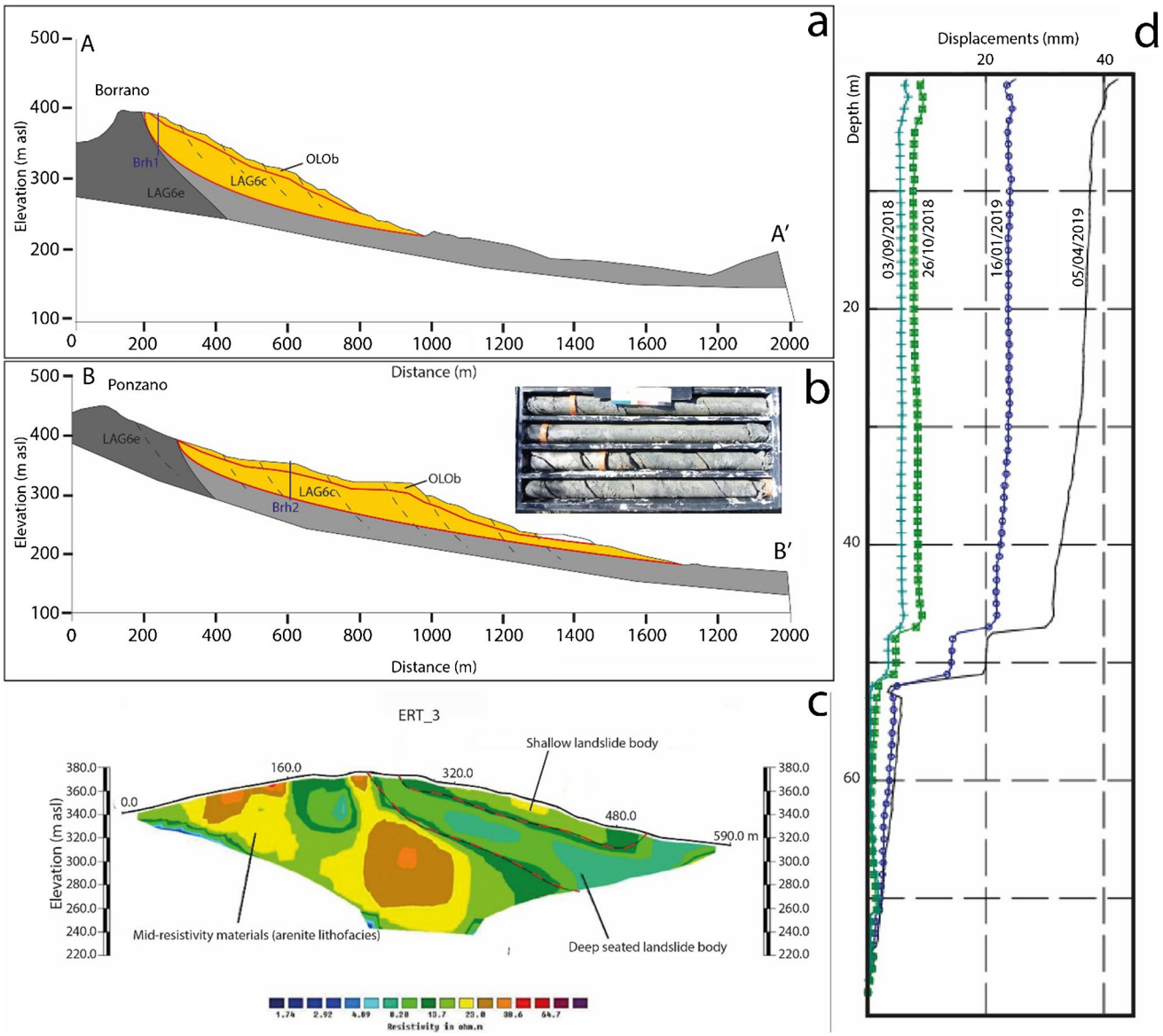

Fig. 7 **a**, **b** depict the geometry of landslides along the geological cross-section A-A′ and B-B′. Red lines depict the position and geometry of the basal and internal shear surfaces. **c**, **d** are examples of geophysical and inclinometric data interpreted in the context of the Borrano and Ponzano landslide analysis

cases, PS groups are related to the presence of buildings affected by the landslides.

Figure 9 shows time series derived by a combination of the ascending and descending displacement rates. Overall, time series indicate that the Borrano landslide moved generally faster than the Ponzano landslide, with maximum values of ~ 40 mm/yr and ~ 12 mm/yr, respectively. The vertical component of the displacement (D_z) is always dominant compared to the horizontal ones (D_x; Fig. 9), and at the upper sector of the Borrano landslide, the movement is characterized by a complete vertical motion. While the upper sector of the Borrano landslide moves faster than its central sector, the upper sector of the Ponzano landslide moves slower than its central sector. For both landslides, a change in landslide velocity is generally observable after mid-2016. It is important to notice that while these data provide a comprehensive overview of the kinematics of the Borrano landslide, the Ponzano landslide failed catastrophically on February 12, 2017, and this evolution is not consistently tracked by PS data due to intrinsic limitation of the DInSAR technique. So only an overview of the kinematics of the Ponzano landslide prior and after the failure is provided (Fig. 9). In this context, it is worth noting that since the term "failure" is used herein to describe the evolution of the landslide mechanism from a stationary creep to a slide dominated, post-failure movement of the Ponzano landslide can be described as a residual movement diffused within the landslide mass and controlled by hydrologic forcing.

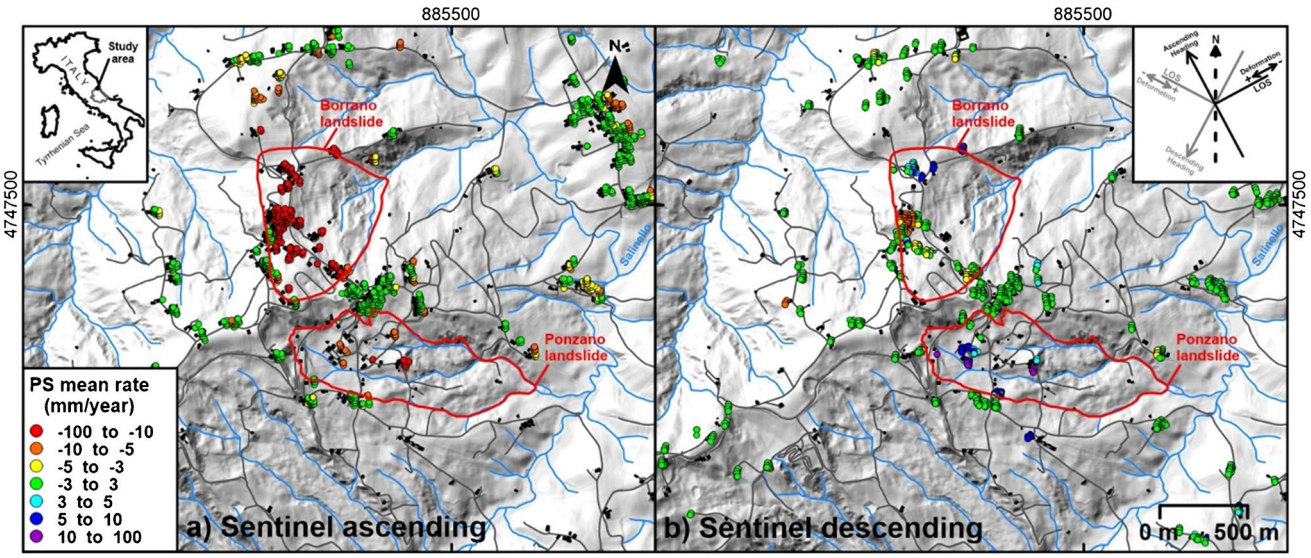

Fig. 8 Maps showing spatial distribution of available EGMS PS (2015–2022) over the Borrano and Ponzano landslides

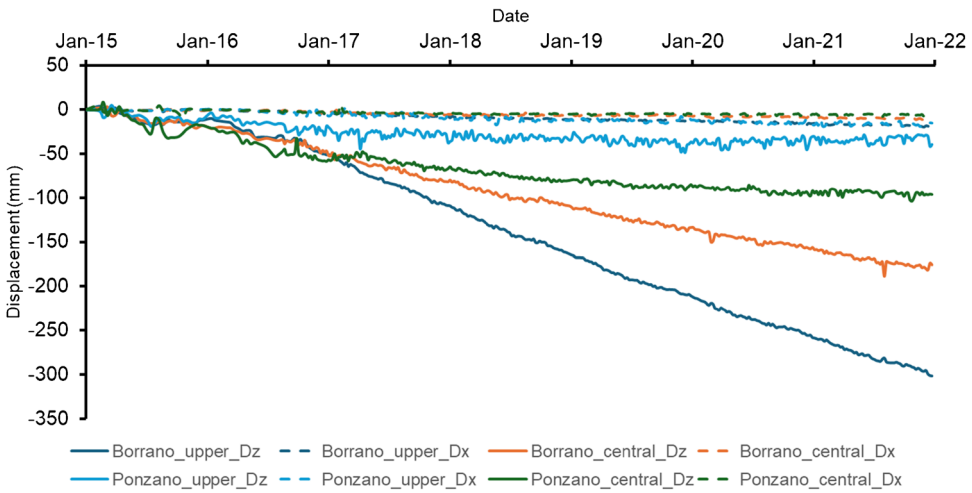

Fig. 9 Time series of vertical (D_z) and horizontal (D_x) displacement derived averaging data from groups of PS identified at significant locations of the Borrano and Ponzano landslides (i.e., upper and central sectors)

Displacement and velocity at Ponzano during the failure of February 12, 2017

Figure 10 shows results from feature tracking over the study area between 2016–01-07 and 2017–12-22 in terms of total displacement. Detectable motion was consistent with a single, brief slip event. As observable from Fig. 10, the algorithm captured the motion of the Ponzano landslide as well as a number of minor deformation events potentially related to additional shallow landslides and/or local acceleration of the Borrano landslide. At Ponzano, higher displacements were estimated at its upper and central sectors, with a maximum of ~ 20 m registered along its axis at ~ 300 m asl. Overall, the spatial distribution of total displacement within the landslide area indicates a typical cross-sectional convex upward profile, with a consistent decrease of total displacement approaching landslide margins, and an axial longitudinal profile characterized by an upper zone of total displacement higher than 15 m and a gradual decrease to less than 5 m below 260 m asl. At Borrano, only a local displacement of ~ 2 m was identified.

Landslide velocity change in relation to earthquakes and rainfall events

Figures 11 and 12 show time series of components of vertical and horizontal cumulative displacement resulting from STL decomposition, depicting the behavior of the Borrano and Ponzano landslides, respectively. Overall, a major breakpoint is recognizable from the time series of the displacement trend for both components of the movement and for both landslides. This breakpoint approximately occurs between August 16 and September 16, 2016, a timeframe in

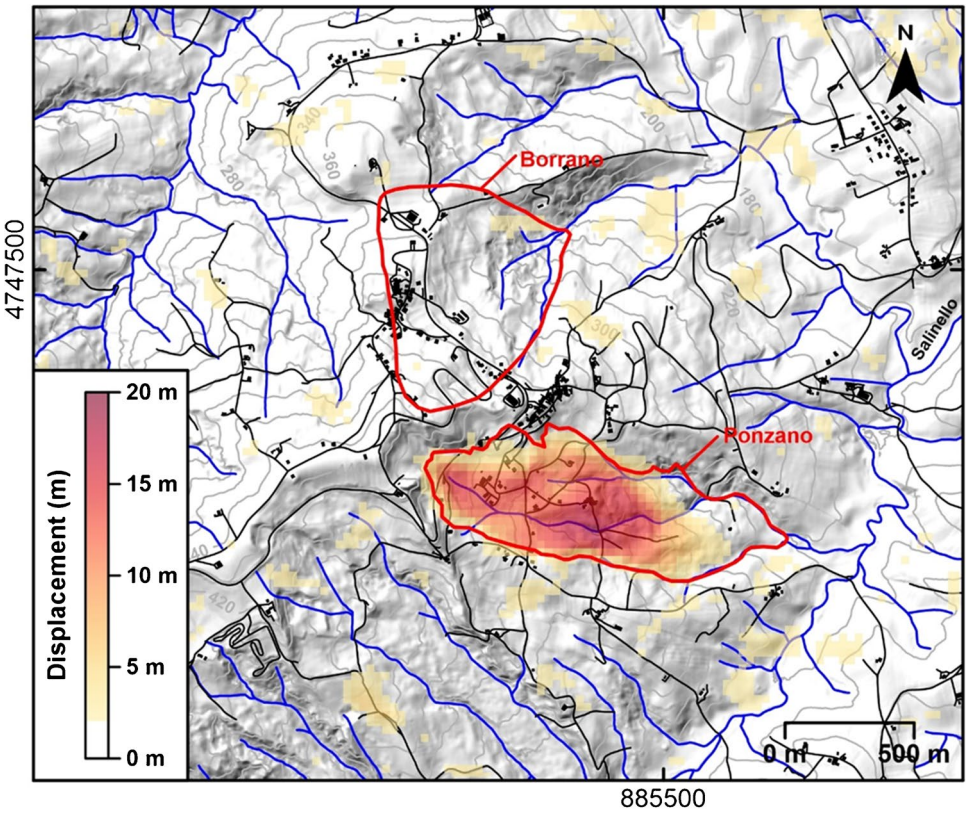

Fig. 10 Map showing results from feature tracking in terms of median surface displacement distribution over the study area between 2016–01-07 and 2017–12-22

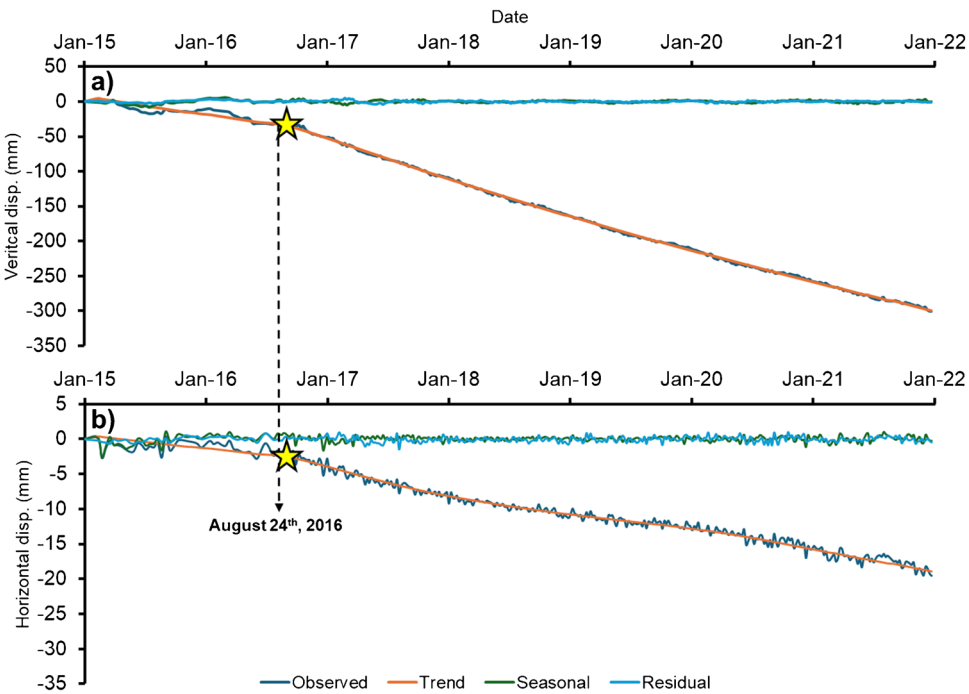

Fig. 11 Results of STL decomposition analysis of time series of **a** vertical and **b** horizontal displacement at the upper sector of the Borrano landslide. Major breakpoint is marked by dashed arrow and associated timing of occurrence. The yellow star indicates timing for major acceleration of the landslide. The dashed line indicates the timing of occurrence of the earthquake

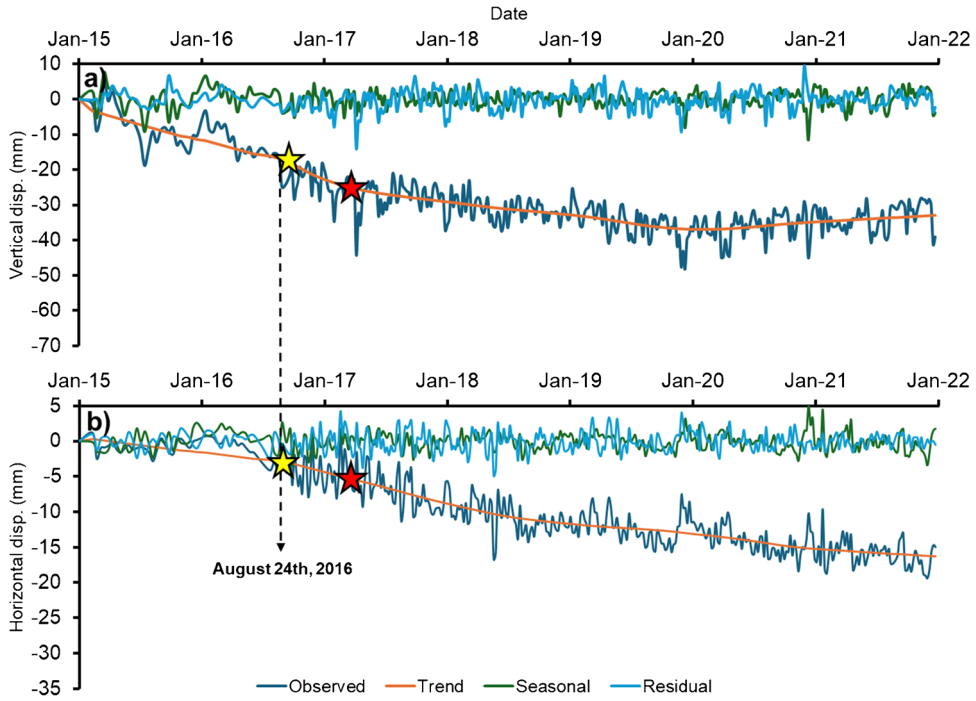

Fig. 12 Results of STL analysis of time series of **a** vertical and **b** horizontal displacement at the upper sector of the Ponzano landslide. Major breakpoint is marked by dashed arrow and associated timing of occurrence. The yellow star indicates timing for major acceleration, and the red star indicates timing of occurrence of the landslide failure. The dashed line indicates the timing of occurrence of the earthquake

which the first Ms = 6.0 earthquake of the 2016–2017 earthquake sequence of central Italy occurred. At Ponzano, a minor breakpoint corresponds to the occurrence of the catastrophic failure of February 2017. For both landslides, the change in velocity (i.e., trend slope) is more significant for the vertical components of the movement, and the Borrano landslide exhibits a higher magnitude change in comparison to Ponzano. Figure 13 depicts the time series of monthly rainfall acquired at the Civitella del Tronto station between January 2016 and January 2018 and considered for the analysis of the factors controlling landslide kinematics. Statistical contextualization of monthly data, through comparison with the long-term mean, indicates how in 2016 cumulative rainfall exceeded the long-term monthly mean in 6 months and the monthly mean plus two standard deviations in June and July. The exceedance of the monthly mean plus two standard deviations occurred approximately from 2 to 3 months before the occurrence of the first Ms = 6.0 earthquake of the 2016–2017 earthquake sequence and observed landslides acceleration. In 2017, monthly rainfall exceeded the long-term monthly mean in January and February, immediately before and in correspondence with the failure of the Ponzano landslide.

Discussion

The engineering-geological model, developed for both landslide areas, highlighted that the Borrano and Ponzano landslides have very similar geotechnical and geological characteristics, with two main sliding surfaces located at ca 10–15 m and 40–50 m of depth, respectively. This agrees with previous studies carried out on the area (Calista et al. 2019). Considering the geological sections (Fig. 7), the landslide crown is located at the contact between two different Laga Formation lithofacies LAG6e and LAG6c. The first displacement surface, at a depth of 10–15 m, is located at the contact between the eluvial deposits and the bedrock (LAG6c), while the deep-seated deformation occurs (ca 40–50 m) within the LAG6c. Results from the satellite analyses indicated that both the Borrano and Ponzano deep-seated landslides consistently moved between 2015 and 2022 with a major slip event of the Ponzano landslide early in 2017. At the upper sector of both landslides, the vertical component of the movement dominated over the horizontal component, suggesting a rotational slide mechanism (Cascini et al. 2010; Hungr et al. 2014). This is also consistent with locally available inclinometric monitoring data at both Borrano and Ponzano, indicating the existence of two sliding surfaces (or a few meter-thick band of distributed shear) at ca 15 and 40 m depth, respectively. More in detail, the results of STL analysis of time series (Figs. 11 and 12) show that both landslides have acceleration starting from September 2016. Such acceleration can be linked with the Central Italy seismic sequence occurred ~ 40 km far from the landslides on August 24, 2016, with a Ms = 6.0. While the Borrano landslide exhibited a persistent slow movement from September 2016 till now, the Ponzano landslide failed in February 2017. The slip event of the Ponzano landslide (with displacements rate of meters per day), however, is not visible in the STL data, which highlights a similar constant movement of both landslides. This is related to the very well-known limitation of the DInSAR analyses of capturing high displacements. Due to this, in this research, the DInSAR data have been coupled with an innovative and recently developed feature tracking analysis. Feature tracking analyses, diversely from DInSAR, are able to detect high rate displacements, which in the case of the Ponzano landslide

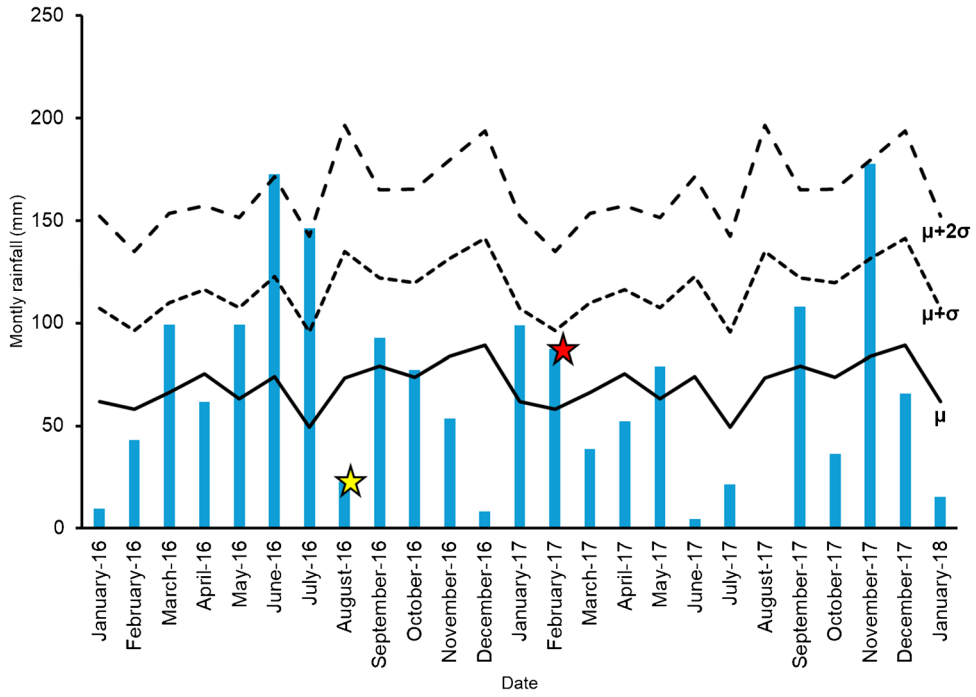

Fig. 13 Statistical significance of monthly rainfall registered at the Civitella del Tronto station. Lines in the graph depict monthly-estimated long-term mean (μ), mean plus one standard deviation (μ + σ; i.e., 68th percentile of a normal distribution) and mean plus two standard deviations (μ + 2σ; i.e., 95th percentile of a normal distribution). The yellow star indicates timing for major acceleration of the landslides, and the red star indicates timing of occurrence of the landslide failure at Ponzano

reached up to 20 m. The DInSAR and feature tracking studies have been integrated with the analysis of monthly rainfall using Civitella del Tronto station. Such data point out that monthly rainfall exceeded (in both landslide areas) the long-term monthly mean in January and February 2017, immediately before and in correspondence of the failure of the Ponzano landslide. In this context, it can be hypothesized that the 2016 seismic sequence and the heavy rainfall occurred in June and July 2016 might have been responsible for the acceleration of both landslides. Furthermore, the slightly above mean rainfall of January and February 2017 might have contributed to the catastrophic failure of the Ponzano landslide. However, it is still difficult to correlate this slightly above mean rainfall to the failure of Ponzano landslide. In fact, the same rainfall occurred in the Borrano area, with no evidence of acceleration of the Borrano landslide. Indeed, seismic shaking has been recognized as a modulation factor for landslide motion during and after earthquakes (Lacroix et al. 2014, 2020), and landslide velocity change has been related to a number of potential mechanisms, including transient increase in shear stress and change in landslide material properties (Jibson et al. 1994; Wasowski et al. 2002; Grelle and Guadagno 2010; Lacroix et al. 2015), which might be consistent with the characteristics of the Borrano and Ponzano landslides. In addition, the potential for the August 24, 2016, earthquake to induce an acceleration of both landslides can be speculated considering the source-to-site–magnitude envelopes proposed by Keefer (1984) and extended by Rodríguez et al. (1999) for coherent landslides, where the combination of source-to-site and magnitude characterizing the Borrano and Ponzano landslide lies at the edge of the envelope.

Explaining the post-seismic behavior of the Ponzano landslides, which failed catastrophically approximately 6 months after the recorded acceleration, is more challenging since mechanisms and factors regulating post-seismic landslide motion are only partially understood, also as a consequence of the frequent lack of correlation between co-seismic and post-seismic displacements. Depending on the scale of delay, post-seismic landslide motion can be influenced by co-seismic weakening of landslide materials (Xi et al. 2024) and modulated by a combined action of seismic loading and rainfall infiltration (months to years; Bontemps et al. 2020) or by pore-water pressure generated outside from the basal-shear zone and diffused into that (days to months; Kohler and Puzrin, 2023). On this basis, a potential explanation for the behavior of the Ponzano landslide might be related to the continuous weakening of the landslide material culminating in a sudden failure. This process is often related to the creep behavior of landslide material, represented by a slow movement occurring at relatively constant rate under normal gravitational force (Fleming and Johnson 1975; Emery 1978; Van Asch 1984). In geologic materials, creep behavior is caused by a combination of strain limiting processes and damage accumulation (Cornelius and Scott 1993) and can be considered the geodetic signature of the progressive failure of a slope (e.g. Saito 1965). These materials fail only after the formation of a shear surface as a consequence of the development and growth of microcracks through the slope (Carey and Petley 2014). Movement patterns in creeping landslides are directly related to brittle or ductile deformation regimes occurring at or near the base of the unstable mass. Brittle mechanics generally determines the sudden failure of

slope after a short period of slow movement. Ductile materials generally display longer-term slow movement, and failure occurs only in the presence of a sustained change in boundary conditions (e.g., external load). In these circumstances, slow movement anticipating failure occurs at relatively constant rate tending to accelerate prior to failure (e.g., Petley and Allison 1997). The characteristics of the material of the Borrano and Ponzano landslides and the observation of their kinematics suggest a ductile behavior of the fine-grained landslide material with the August 24, 2016, earthquake responsible for the change in boundary conditions driving the failure of the Ponzano landslide. Although this might be an explanation for this behavior, a hyperbolic increase of landslide velocity was not observable from available data, probably because of the intrinsic limitation of DInSAR time series and the low temporal resolution of feature tracking analysis in relation to image acquisition frequency. The absence of the same behavior for the Borrano landslide might be interpreted in the context of the global stability conditions of the slope. Indeed, the progressive failure model proposed by Petley et al. (2005) assumed that final failure of creeping landslides occurs when the factor of safety equals unity. On this basis, a hypothesis might be that the global stability conditions of the Borrano landslide correspond to a factor of safety higher than that characterizing the Ponzano landslide during the summer 2016. Overall, this condition might be also related to the age of the landslide with the Borrano landslide that might be younger than the Ponzano landslide. A further hypothesis can be related to the geometry of the slope that in the case of the Borrano landslide might be not favorable to catastrophic evolution. On this basis, a major question that might arise deals with the effective opportunity of using insights from the Ponzano landslide to better understand and potentially predict the prospective behavior of the Borrano landslide. The prospective behavior of the Borrano landslide is consistently related, not only to the seasonal or transient variations in both the driving and resisting forces, but also to the characteristics of the involved materials (e.g., in terms of time-dependent behavior) and its three-dimensional geometry. In these conditions, long-term weakening, identified as potential driving factors for landslide failure at Ponzano, might effectively sustain an eventual catastrophic evolution at Borrano, but considering the ductile nature of the involved materials, this would be expected as a result of a significant transient perturbation (e.g., earthquake, extremely wet period) or, alternatively, over a very long term.

Conclusions

The Ponzano and Borrano landslides affect slopes characterized by similar geological and geotechnical settings. Concave upward basal slip surfaces have been identified in both landslides at ~ 15 and 40 m of depth, respectively. The shallower surface represents the contact between eluvial-colluvial deposits and the bedrock, while the deeper surface is located within the Laga formation. The geometry of the landslide has been reconstructed by combining LiDAR and UAV data, data from borehole inclinometers, and field geological/geomorphological observations. Results from DInSAR data analysis indicated that both landslides consistently moved between 2015 and 2022 with a major slip event of the Ponzano landslide early in 2017. At the upper sector of both landslides, the vertical component of the movement dominated over the horizontal components, thus suggesting a rotational slide mechanism. Time series analysis indicates a major acceleration of both landslides between August and September 2016, a timeframe in which a Ms = 6.0 earthquake of the 2016–2017 earthquake sequence of central Italy occurred. In addition, this acceleration occurred after 2 months of above average rainfall that, in association with the earthquake shaking, might have contributed to perturbate landslide motion. After 6 months from this acceleration, the Ponzano landslide failed catastrophically with no evidence of triggers. A potential explanation for the behavior of the Ponzano landslide might be related to the progressive weakening of the landslide material culminating in a sudden failure. The slip episode induced by the failure of the Ponzano landslide was too rapid for DInSAR detection, so feature tracking had to be applied for unraveling landslide kinematics during failure. Implication from this is that, in case of catastrophic failure of deep-seated landslides, multiple displacement tracking methods need to be integrated to effectively characterize landslide motion. Additionally, insights from the Ponzano landslide might form a basis for predicting the prospective behavior of the Borrano landslide. Long-term weakening, identified as potential driving factors for landslide failure at Ponzano, might effectively sustain an eventual catastrophic evolution also at Borrano, but due to the ductile nature of the involved materials, this would be expected as a result of a significant transient perturbation.

Acknowledgements

The authors thank Emilie Lemaire and an anonymous reviewer for providing constructive reviews of the manuscript.

Funding

The research was partly funded through the BGS International Geoscience Research and Development Programme.

Data Availability

All data used in this work are either publicly available or available from the authors upon request

Declarations

Conflict of interest The authors declare no competing interests.

References

Allasia P, Baldo M, Giordan D, Godone D, Wrzesniak A, Lollino G (2019) Near real time monitoring systems and periodic surveys using a multi sensors UAV: the case of Ponzano landslide. In: Slope stability: case histories, landslide mapping, emerging technologies, Springer International Publishing, pp 303–310

Antonello G, Casagli N, Farina P, Leva D, Nico G, Sieber AJ, Tarchi D (2004) Ground-based SAR interferometry for monitoring mass movements. Landslides 1:21–28

Arai N, Chigira M (2019) Distribution of gravitational slope deformation and deep-seated landslides controlled by thrust faults in the Shimanto accretionary complex. Eng Geol 260:1–18

Baron I, Cilek V, Krejci O, Melichar R, Hubatka F (2004) Structure and dynamics of deep-seated slope failures in the Magura Flysch Nappe, outer Western Carpathians (Czech Republic). Nat Hazards Earth Syst Sci 4:549–562

Baum RL, Fleming RW (1991) Use of longitudinal strain in identifying driving and resisting elements of landslides. Geol Soc Am Bull 103:1121–1132
Bontemps N, Lacroix P, Larose E, Jara J, Taipe E (2020) Rain and small earthquakes maintain a slow-moving landslide in a persistent critical state. Nat Commun 11:780
Booth A, McCarley J, Hinkle J, Shaw S, Ampuero JP, Lamb MP (2018) Transient reactivation of a deep-seated landslide by undrained loading captured with repeat airborne and terrestrial lidar. Geophys Res Lett 45:4841–4850
Břežný M, Pánek T (2017) Deep-seated landslides affecting monoclinal flysch morphostructure: evaluation of LiDAR-derived topography of the highest range of the Czech Carpathians. Geomorphology 285:44–57
Brideau MA, Yan M, Stead D (2009) The role of tectonic damage and brittle rock fracture in development of large rock slope failure. Geomorphology 103:30–49
Calista M, Miccadei E, Piacentini T, Sciarra N (2019) Morphostructural, meteorological and seismic factors controlling landslides in weak rocks: the case studies of Castelnuovo and Ponzano (North East Abruzzo, Central Italy). Geosciences 9:122
Cantalamessa G, Di Celma C (2004) Sequence response to syndepositional regional uplift: insights from high-resolution sequence stratigraphy of late Early Pleistocene strata, Periadriatic Basin, central Italy. Sed Geol 164:283–309
Carboni F, Porreca M, Valerio E, Mariarosaria M, De Luca C, Azzaro S et al (2022) Surface ruptures and off-fault deformation of the October 2016 central Italy earthquakes from DInSAR data. Sci Rep 12:3172
Carey JM, Petley DN (2014) Progressive shear-surface development in cohesive materials; implications for landslide behaviour. Eng Geol 177:54–65
Cascini L, Fornaro G, Peduto D (2010) Advanced low- and full-resolution DInSAR map generation for slow-moving landslide analysis at different scales. Eng Geol 112:29–42
Cevasco A, Termini F, Valentino R, Meisina C, Bonì R, Bordoni M, Chella GP, De Vita P (2018) Residual mechanisms and kinematics of the relict Lemeglio coastal landslide (Liguria, northwestern Italy). Geomorphology 320:64–81
Chen CW, Lida T, Yamada R (2017) Effects of active fault types on earthquake-induceddeep-seated landslides: a study of historical cases in Japan. Geomorphology 295:680–689
Chiaraluce L, Di Stefano R, Tinti E, Scognamiglio L, Michele M, Casarotti E et al (2017) The 2016 central Italy seismic sequence: a first look at the mainshocks, aftershocks, and source models. Seismol Res Lett 88:757–771
Chigira M (2009) September 2005 rain-induced catastrophic rockslides on slopes affected by deep-seated gravitational deformations, Kyushu, southern Japan. Eng Geol 108:1–15
Chigira M, Yagi H (2006) Geological and geomorphological characteristics of landslides triggered by the 2004 Mid Nigata prefecture earthquake in Japan. Eng Geol 82:202–221
Cleveland RB, Cleveland WS, McRae JE, Terpenning I (1990) STL: a seasonal-trend decomposition procedure based on loess. J Off Stat 6:3–73
Colesanti C, Wasowski J (2006) Investigating landslides with space-borne Synthetic Aperture Radar (SAR) interferometry. Eng Geol 88:173–199
Confuorto P, Di Martire D, Centolanza G, Iglesias R, Mallorqui JJ, Novellino A, Plank S, Ramondini M, Thuro K, Calcaterra D (2017) Post-failure evolution analysis of a rainfall-triggered landslide by multi-temporal interferometry SAR approaches integrated with geotechnical analysis. Remote Sens Environ 188:51–72
Cornelius RR, Scott PA (1993) A materials failure relation of accelerating creep as empirical description of damage accumulation. Rock Mech Rock Eng 26:233–252
Crosetto M, Solari L, Balasis-Levinsen J, Bateson L, Casagli N, Frei M et al (2021) Deformation monitoring at European scale: the Copernicus ground motion service. Int Arch Photogramm Remote Sens Spat Inf Sci 43:141–146
Di Martire D, De Luca G, Ramondini M, Calcaterra D (2013) Landslide-related PS data interpretation by means of different techniques. Landslide science and practice. Springer, Berlin Heidelberg, pp 347–355
Di Martire D, Novellino A, Raimondini M, Calcaterra D (2016) A-differential synthetic aperture radar interferometry analysis of a deep seated gravitational slope deformation occurring at Bisaccia (Italy). Sci Total Environ 550:556–573
Di Martire D, Paci M, Confuorto P, Costabile S, Guastaferro F, Verta A, Calcaterra D (2017) A nation-wide system for landslide mapping and risk management in Italy: the second not-ordinary plan of environmental remote sensing. Int J Appl Earth Obs Geoinf 63:143–157
Dille A, Kervyn F, Bibentyo TM, Delvaux D, Ganza GB, Mawe GI et al (2019) Causes and triggers of deep-seated hillslope instability in the tropics–Insights from a 60-year record of Ikoma landslide (DR Congo). Geomorphology 345:106835
Dille A, Kervyn F, Handwerger AL, d'Oreye N, Derauw D, Bibentyo TM et al (2021) When image correlation is needed: unravelling the complex dynamics of a slow-moving landslide in the tropics with dense radar and optical time series. Remote Sens Environ 258:112402
Dille A, Dewitte O, Handwerger AL, d'Oreye N, Derauw D, Ganza Bamulezi G et al (2022) Acceleration of a large deep-seated tropical landslide due to urbanization feedbacks. Nat Geosci 15:1048–1055
Emery JJ (1978) Simulation of slope creep. In: Developments in geotechnical engineering. Elsevier, pp 669–691
Esposito C, Di Luzio E, Baleani M, Troiani F, Della Seta M, Bozzano F, Mazzanti P (2021) Fold architecture predisposing deep-seated gravitational slope deformations within a flysch sequence in the Northern Apennines (Italy). Geomorphology 380:107629
Esu F (1977) Behaviour of slopes in structurally complex formations. In: Proceeding of the International Symposium The Geotechnics of Structurally Complex Formations, pp 292–303
Ferretti A, Prati C, Rocca F (2001) Permanent scatterers in SAR interferometry. IEEE Trans Geosci Remote Sens 39:8–20
Fleming RW, Johnson AM (1975) Rates of seasonal creep of silty clay soil. Q J Eng GeolHydrogeol 8:1–29
Fleming RW, Johnson AM (1989) Structures associated with strike-slip faults that bound landslide elements. Eng Geol 27:39–114
Forte G, Verrucci L, Di Giulio A, De Falco M, Tommasi P, Lanzo G et al (2021) Analysis of major rock slides that occurred during the 2016–2017 Central Italy seismic sequence. Eng Geol 290:106194
Grelle G, Guadagno FM (2010) Shear mechanisms and viscoplastic effects during impulsive shearing. Geotechnique 60:91–103
Guerriero L, Revellino P, Luongo A, Focareta M, Grelle G, Guadagno FM (2016) The Mount Pizzuto earth flow: deformational pattern and recent thrusting evolution. J Maps 12:1187–1194
Guerriero L, Bertello L, Cardozo N, Berti M, Grelle G, Revellino P (2017) Unsteady sediment discharge in earth flows: a case study from the Mount Pizzuto earth flow, southern Italy. Geomorphology 295:260–284
Guerriero L, Confuorto P, Calcaterra D, Guadagno FM, Revellino P, Di Martire D (2019) PS-driven inventory of town-damaging landslides in the Benevento, Avellino and Salerno Provinces, southern Italy. J Maps 15:619–625
Guerriero L, Di Martire D, Calcaterra D, Francioni M (2020) Digital image correlation of Google Earth images for Earth's surface displacement estimation. Remote Sens 12:3518
Guerriero L, Prinzi EP, Calcaterra D, Ciarcia S, Di Martire D, Guadagno FM et al (2021) Kinematics and geologic control of the deep-seated landslide affecting the historic center of Buonalbergo, southern Italy. Geomorphology 394:107961
Guerriero L, Ruzza G, Calcaterra D, Guadagno FM, Revellino P (2022) Accelerating creep in deep-seated landslides moving along clay layers. Riv Ital Geotecnica 2(2022):49–53
Handwerger AL, Roering JJ, Schmidt DA (2015) Controls on the seasonal deformation of slow-moving landslides. Earth Planet Sci Lett 377:239–247
Hungr O, Leroueil S, Picarelli L (2014) The Varnes classification of landslide types, an update. Landslides 11:167–194
Iverson RM (2000) Landslide triggering by rain infiltration. Water Resour Res 36:1897–1910
Iverson RM (2005) Regulation of landslide motion by dilatancy and pore pressure feedback. J Geophys Res Earth Surf 110:1–16
Iverson RM, Major JJ (1987) Rainfall, ground-water flow, and seasonal movement at Minor Creek landslide, northwestern California: physical interpretation of empirical relations. Geol Soc Am Bull 99:579–594
Jiang S, Wang Y, Tang C, Liu K (2018) Long-term kinematics and mechanism of a deepseated slow-moving debris slide near Wudongde hydropower station in Southwest China. J Mt Sci 15:364–379
Jibson RW, Prentice CS, Borissoff BA, Rogozhin EA, Langer CJ (1994) Some observations of landslides triggered by the 29 April 1991 Racha earthquake, Republic of Georgia. Bull Seismol Soc Am 84:963–973

Keefer DK (1984) Landslides caused by earthquakes. Geol Soc Am Bull 95:406–421
Kohler M, Puzrin AM (2023) Mechanics of coseismic and postseismic acceleration of active landslides. Commun Earth Environ 4:122
Kojima S, Nagata H, Yamashiroya S, Iwamoto N, Ohtani T (2015) Large deep-seated landslides controlled by geologic structures: prehistoric and modern examples in a Jurassic subduction–accretion complex on the Kii Peninsula, central Japan. Eng Geol 186:44–56
Lacroix P, Perfettini H, Taipe E, Guillier B (2014) Coseismic and postseismic motion of a landslide: observations, modeling, and analogy with tectonic faults. Geophys Res Lett 41:6676–6680
Lacroix P, Berthier E, Maquerhua ET (2015) Earthquake-driven acceleration of slow-moving landslides in the Colca valley, Peru, detected from Pléiades images. Remote Sens Environ 165:148–158
Lacroix P, Handwerger AL, Bièvre G (2020) Life and death of slow-moving landslides. Nat Rev Earth Environ 1:404–419
Manconi A (2021) How phase aliasing limits systematic space-borne DInSAR monitoring and failure forecast of alpine landslides. Eng Geol 287:106094
Martino S, Moscatelli M, Scarascia Mugnozza G (2004) Quaternary mass movements controlled by a structurally complex setting in the central Apennines (Italy). Eng Geol 72:33–55
Martino S, Bozzano F, Caporossi P, D'angiò D, Della Seta M, Esposito C et al (2019) Impact of landslides on transportation routes during the 2016–2017 Central Italy seismic sequence. Landslides 16:1221–1241
Meletti C, Marzocchi W, D'Amico V, Lanzano G, Luzi L, Martinelli F, Pace B, Rovida A, Taroni M, Visini F, MPS19 Working Group (2021) The new Italian seismic hazard model (MPS19). Ann Geophys 64:SE112
Newmark NM (1965) Effects of earthquakes on dams and embankments. Geotechnique 15:139–160
Nguyen LC, Tien PV, Do TN (2020) Deep-seated rainfall-induced landslides on a new expressway: a case study in Vietnam. Landslides 17:395–407
Pappalardo G, Mineo S, Angrisani AC, Di Martire D, Calcaterra D (2018) Combining field data with infrared thermography and DInSAR surveys to evaluate the activity of landslides: the case study of Randazzo Landslide (NE Sicily). Landslides 15:2173–2193
Petley DN, Allison RJ (1997) The mechanics of deep-seated landslides. Earth Surf Proc Land 22:747–758
Petley DN, Higuchi T, Petley DJ, Bulmer MH, Carey J (2005) Development of progressive landslide failure in cohesive materials. Geology 33:201–204
Pinto F, Guerriero L, Revellino P, Grelle G, Senatore MR, Guadagno FM (2016) Structural and lithostratigraphic controls of earthflow evolution, Montaguto earth flow, Southern Italy. J Geol Soc 173:649–665
Rodrıguez CE, Bommer JJ, Chandler RJ (1999) Earthquake-induced landslides: 1980–1997. Soil Dyn Earthq Eng 18:325–346
Roering JJ, Kirchner JW, Dietrich WE (2005) Characterizing structural and lithologic controls on deep-seated landsliding: implication for topographic relief and landscape evolution in the Oregon Coastal Range, USA. Bull Geol Soc Am 117:654–668
Rygus M, Novellino A, Hussain E, Syafiudin F, Andreas H, Meisina C (2023) A clustering approach for the analysis of InSAR time series: application to the Bandung basin (Indonesia). Remote Sensing 15:3776
Saito M (1965) Forecasting the time of occurrence of a slope failure. In: Proceedings of the 6th International Conference of Soil Mechanics and Foundation Engineering, pp 537–541
Sassa K, Fukuoka H, Scarascia Mugnozza G, Evans S (1996) Earthquake-induced-landslides: distribution, motion and mechanisms. Soils Found 36:53–64
Schlögel R, Doubre C, Malet JP, Masson F (2015) Landslide deformation monitoring with ALOS/PALSAR imagery: a D-InSAR geomorphological interpretation method. Geomorphology 231:314–330
Schulz WH, McKenna JP, Kibler JD, Biavati G (2009) Relations between hydrology and velocity of a continuously moving landslide—evidence of pore-pressure feedback regulating landslide motion? Landslides 6:181–190
Schulz WH, Coe JA, Ricci PP, Smoczyk GM, Shurtleff BL, Panosky J (2017) Landslide kinematics and their potential controls from hourly to decadal timescales: insights from integrating ground-based InSAR measurements with structural maps and long-term monitoring data. Geomorphology 285:121–136
Solari L, Raspini F, Del Soldato M, Bianchini S, Ciampalini A, Ferrigno F et al (2018) Satellite radar data for back-analyzing a landslide event: the Ponzano (Central Italy) case study. Landslides 15:773–782
Squarzoni G, Bayer B, Franceschini S, Simoni A (2020) Pre-and post-failure dynamics of landslides in the Northern Apennines revealed by space-borne synthetic aperture radar interferometry (InSAR). Geomorphology 369:107353
Stumpf A, Malet JP, Delacourt C (2017) Correlation of satellite image time-series for the detection and monitoring of slow-moving landslides. Remote Sens Environ 189:40–55
Sun HY, Zhao Y, Shang YQ, Yu Y, Zhao QL (2012) Deep-seated slope failures induced by inappropriate cutting in China. Rock Mech Rock Eng 45:1103–1111
Van Asch TW (1984) Creep processes in landslides. Earth Surf Proc Land 9:573–583
Van Asch TWJ, Malet JP, Bogaard TA (2009) The effect of groundwater fluctuations on the velocity pattern of slow-moving landslides. Nat Hazards Earth Syst Sci 9:739–749
Van Wyk de Vries M, Ito E, Shapley M, Brignone G (2021) Semi-automated counting of complex varves through image autocorrelation: an open-source toolbox. Quatern Res 104:89–100
Van Wyk de Vries M, Wickert A (2021) Glacier Image Velocimetry: an open-source toolbox for easy and rapid calculation of high-resolution glacier-velocity fields. Cryosphere 2020:1–21
Van Wyk de Vries M, Arrell K, Basyal GK, Densmore AL, Dunant A, Harvey EL et al (2024) Detection of slow-moving landslides through automated monitoring of surface deformation using Sentinel-2 satellite imagery. Earth Surf Proc Land 49:1397–1410
Wasowski J, Pierri V, Pierri P, Capolongo D (2002) Factors controlling seismic susceptibility of the Sele valley slopes: the case of the 1980 Irpinia earthquake re-examined. Surv Geophys 23:563–593
Xi C, Lombardo L, Hu X, Tanyas H (2024) Co-seismic hillslope weakening. Eng Geol 338:107607
Zhi M, Shang Y, Zhao Y, Lü Q, Sun H (2016) Investigation and monitoring on a rainfall-induced deep-seated landslide. Arab J Geosci 9:1–13

Luigi Guerriero (✉) · Domenico Calcaterra · Diego Di Martire
Department of Earth, Environmental and Resource Sciences, Federico II University of Naples, Naples, Italy
Email: luigi.guerriero2@unina.it

Maximillian Van Wyk de Vries
Department of Geography, University of Cambridge, Cambridge, UK

Maximillian Van Wyk de Vries
Department of Earth Sciences, University of Cambridge, Cambridge, UK

Holly Hourston · Alessandro Novellino
British Geological Survey, Environmental Science Centre, Keyworth, Nottingham, UK

Nicola Sciarra
Department of Sciences, Gabriele D'Annunzio University of Chieti-Pescara, Chieti, Italy

Mirko Francioni
Department of Pure and Applied Sciences, Carlo Bo University of Urbino, Urbino, Italy